BBA - Biomembranes 1864 (2022) 183808

Contents lists available at ScienceDirect

BBA - Biomembranes

journal homepage: www.elsevier.com/locate/bbamem

Compositional, structural and functional properties of discrete coexisting complexes within bronchoalveolar pulmonary surfactant

José Carlos Castillo-Sánchez, Alejandro Cerrada, Mikel Conde, Antonio Cruz *, Jesús Pérez-Gil

Department of Biochemistry and Molecular Biology, Faculty of Biology, and Research Institute "Hospital 12 de Octubre (imas12)", Complutense University, Madrid, Spain

ARTICLE INFO

Keywords:
Lung surfactant
Air-liquid interface
Respiratory dynamics
Membrane structure
DSC
ESR

ABSTRACT

Lung surfactant (LS) stabilizes the respiratory surface by forming a film at the alveolar air-liquid interface that reduces surface tension and minimizes the work of breathing. Typically, this surface-active agent has been isolated from animal lungs both for research and biomedical applications. However, these materials are constituted by complex membranous architectures including surface-active and inactive lipid/protein assemblies. In this work, we describe the composition, structure and surface activity of discrete membranous entities that are part of a LS preparation isolated from bronchoalveolar lavages of porcine lungs. Seven different fractions could be resolved from whole surfactant subjected to sucrose density gradient centrifugation. Detailed compositional characterization revealed differences in protein and cholesterol content but no distinct saturated:unsaturated phosphatidylcholine ratios. Moreover, no significant differences were detected regarding apparent hydration at the headgroup region of membranes, as reported by the probe Laurdan, and lipid chain mobility analysed by electron spin resonance (ESR) in spite of the variety of membranous assemblies observed by transmission electron microscopy. In addition, six of the seven separated LS subfractions formed similar, essentially disordered-like, interfacial films and performed efficient surface activity, under physiologically relevant conditions. Altogether, our work show that a LS isolated from porcine lungs is comprised by a heterogenous population of membranous assemblies lacking freshly secreted unused LS complexes sustaining highly dehydrated and ordered membranous assemblies as previously reported. We propose that surfactant subfractions may illustrate intermediates in sequential structural steps within the structural transformations occurring along the respiratory compression-expansion cycles.

1. Introduction

Surface tension (γ) forces generated at the alveolar air-liquid interface are balanced out by Lung Surfactant (LS), and this facilitates the dynamic effort of breathing [1]. This surface-active material is mainly composed by lipids, comprising more than 90% of surfactant by mass [1]. In this regard, dipalmitoyl-phosphatidylcholine (DPPC), which accounts for 40% (w), allows diminishing γ to minimal values upon the compression of the respiratory surface that occurs at the end of expiration. In addition, LS contains anionic phospholipids such as phosphatidylinositol and phosphatidylglycerol that establish ionic interactions with hydrophobic surfactant proteins [1]. Furthermore, 5% of surfactant mass is cholesterol, whose levels are tightly regulated to modulate lipid phase coexistence [2]. As a matter of fact, increased cholesterol levels may alter the surface activity of LS [3]. Apart from lipids, the protein fraction of LS, which accounts for about 10% (w), includes hydrophilic surfactant proteins A (SP-A) and D (SP-D), involved in innate immunity, and hydrophobic surfactant proteins B (SP-B) and C (SP-C) that play key roles to optimize the surface activity of LS [1].

To fulfil its main function, LS is considered to form an oriented monolayer once adsorbed into the respiratory air-liquid interface. However, the lipid/protein complexes of LS are involved in a highly regulated bio-structural cycle from its synthesis and secretion into the airspaces to its recycling [4]. Firstly, surfactant lipids and proteins SP-B and SP-C are jointly packed by type II pneumocytes as highly dehydrated multilamellar arrays in specialized organelles called lamellar bodies (LBs) [4–6]. After secretion, LBs disintegrate at the air-liquid interface and transfer their surface-active constituents to form the surface film

* Corresponding author at: Departamento de Bioquímica y Biología Molecular, Facultad de Biología, Universidad Complutense de Madrid, José Antonio Novais 12, 28040 Madrid, Spain.
E-mail addresses: josecarc@ucm.es (J.C. Castillo-Sánchez), acerrada@ucm.es (A. Cerrada), acruz@ucm.es (A. Cruz), jperezgil@bio.ucm.es (J. Pérez-Gil).

https://doi.org/10.1016/j.bbamem.2021.183808
Received 29 July 2021; Received in revised form 10 October 2021; Accepted 11 October 2021
Available online 20 October 2021

[7]. A fraction of LBs unpack into intermediate membranous assemblies such as tubular myelin [8]. As a result of surface dynamics, inactive aggregates are continuously generated and recycled by type II pneumocytes and alveolar macrophages [4]. The uptake of wasted material is somehow coordinated with surfactant secretion in processes that are at least partially modulated by surfactant proteins [9,10].

The quantification and characterization of the different membranous assemblies taking part of LS has been a matter of research along the years [11–17]. In this line, LS complexes isolated from bronchoalveolar lavages of animal lungs were proposed to include surface-active (large aggregates) and inactive constituents (small aggregates). Large aggregates are thought to be precursors of small aggregates inasmuch as their exposure to surface cycling result in conversion to small aggregates [14]. In addition, their levels may be altered under pathological conditions such as abnormal respiratory rates, acute lung injury or pneumonitis [18–22].

Beyond the distinction between large and small aggregates, the structure and lipid/protein interactions in several membranous entities included into or derived from LS have been described in the recent years. This is the case of LBs [5,6,23], lamellar body-like particles (LBPs) [5,6,24], tubular myelin [25], interfacial monolayers [26–28], multibilayer stacks [29,30] and lipid-based giant vesicles [2]. As a matter of fact, those sub-structures are thought to differ each other in terms of composition, lipid phase segregation, lipid polymorphism and level of hydration, all factors with critical impact in the surface activity of LS [1]. On the other hand, recent studies have also revealed that the structure and thermotropic behaviour of surfactant isolated from lavages differs substantially from the behaviour of surfactant freshly secreted by primary cultures of type II pneumocytes [5]. To what extent the surfactant from whole bronchoalveolar lavage contains a fraction of freshly secreted surfactant that could be comparable to that secreted by cultured cells has not been studied. To shed light on the structure-function relationships in the membranous architecture of LS, this work presents a detailed description of the composition, structure and surface-activity of LS subfractions.

2. Materials and methods

2.1. Isolation of LS subfractions

LS complexes were isolated from bronchoalveolar lavages of porcine lungs obtained from the slaughterhouse. To do so, respiratory tracts were washed with a buffer solution containing Tris 5 mM, NaCl 150 mM and pH 7. Then, cellular debris were removed by a short centrifugation (1000 *g*, 5 min at 4 °C). Afterwards, membranes were pelleted by centrifugation for 1 h at 100000 *g* at 4 °C. After that, pellets were homogenized and loaded into sodium bromide density gradients containing (from bottom to the top): 4 ml of NaBr 16% (w/v) in NaCl 0.9%; 6 ml NaBr 13% in NaCl 0.9%; and 2.5 ml NaCl 0.9%. After centrifugation for 2 h at 120000 *g* and 4 °C, the so-called whole LS was harvested from the interface between the second and third gradient solutions. To obtain LS subfractions, we followed a protocol previously described in the literature [31]. Isolated LS complexes were loaded into density gradients constituted by sucrose solutions at 0.9, 0.8, 0.7, 0.55, 0.45 and 0.32 M. Then, density gradients were centrifuged for 2 h at 120000 *g* and 4 °C.

2.2. Compositional analyses

Phospholipid concentration was determined by phosphorus quantification upon mineralization of the phosphate group [32]. The quantification of saturated and unsaturated molecular species of phosphatidylcholine was conducted in the Research Unit on Bioactive Molecules (IQAC-CSIC), with the collaboration of Drs. Josefina Casas and Gemma Fabrias, as previously described [33]. Cholesterol levels were measured using a commercial kit (Spinreact, Barcelona), which is based on coupled reactions to produce a quinonimine that is quantified by its absorbance at 505 nm [34].

Acrylamide gels at 16 and 10% were used for western blot analyses in order to detect the presence of proteins SP-B and SP-C or SP-A respectively. Equal phospholipid amounts were loaded per well (10 μg for SP-A and SP-C and 5 μg for SP-B). Antibodies employed were: αSP-A (dilution 1/10000) kindly provided by Prof. David Phelps, Department of Paediatrics, University of Pennsylvania at Hershey, USA; αSP-B and αSP-C (dilutions 1/5000) from Seven Hills Bioreagents (Cincinnati); and rabbit anti-immunoglobulins (dilution 1/5000, Dako). ECL Immobilon Western from Millipore was used for revealing in an image analyser (Image Quant-Las 500, GE, Healthcare Bio-sciences AB).

2.3. Transmission electron microscopy (TEM)

Surfactant suspensions were centrifuged and pellets were fixed by incubation with glutaraldehyde for 5 h at 4 °C. Then, samples were treated with 1% osmium tetra-oxide for 1 h. Afterwards, samples were dehydrated with increasing concentrated acetone solutions and embedded in Spurr resin. Finally, sections of the embedded resin were observed in a JEOL, JEM1010 model, electron microscopy located at the National Centre of Microscopy (Madrid, Spain).

2.4. Laurdan fluorescence

Membrane hydration was evaluated using the fluorescence probe Laurdan as described previously in the literature [35,36]. For labelling, Laurdan (D250 from ThermoFisher Scientific) was solved in a trace of dimethyl sulfoxide and added to surfactant suspensions at 10 μg/ml to get a final dye proportion of 1% (mol/mol with respect to phospholipid). Then, samples were stored in a dark chamber at room temperature for 30 min to complete Laurdan incorporation and equilibration. Finally, fluorescence emission spectra ($\lambda_{excitation} = 370$ nm) were recorded from the samples from 400 to 550 nm at 10, 15, 20, 25, 30, 35, 37, 40, 45, 50 and 55 °C. Generalized Polarization Function of Laurdan (GPF) was calculated according to the following equation: $GPF = (I_{440} - I_{490}) / (I_{440} + I_{490})$, where I_{440} and I_{490} are the fluorescence emission intensity of the samples at 440 and 490 nm.

2.5. Electron spin resonance

Acyl chain mobility of the phospholipids in the different surfactant assemblies was evaluated by electron spin resonance as described previously for the study of LS membranes [37,38]. To this purpose, surfactant membranes were labelled with 5 and 12-DOXYL-phosphatydylcholine spin labels (5 and 12-PCSL, from Avanti Polar Lipids) at room temperature. After that, samples were loaded into micro-Haematocrit tubes (Catalog number 7493 11, from Brand GMBH) and centrifuged with a Haematocrit-Rotor (ThermoFisher Scientific) at 21000 g, 4 °C for 30 min. Haematocrit tubes were introduced into quartz tubes with silicon oil for thermal stability. Then, ESR spectra were recorded at the Research Support Center in Complutense University (Madrid, Spain) using a Bruker EMX 10/12 Spectrometer fitted with a nitrogen flow temperature regulation system. Two spectra were recorded per temperature (25, 30, 37 and 45 °C) and sample to minimize noise during acquisition. WinEPR software was employed for recordings. Settings were: 10 mW microwave power, 1.25 G modulation amplitude, 100 kHz modulation frequency, 0.33 s time constant, 150 G sweep width and 3360 center field.

2.6. Differential scanning calorimetry

Surfactant suspensions were prepared at a phospholipid concentration of 1 mg/ml in Tris 5 mM, NaCl 150 mM pH 7. Thermograms were acquired at a scan rate of 30 °C/h in a microcalorimeter MicroCal VP-DSC. 15 scans between 15 and 60 °C were recorded. Origin 7 (OriginLab Corporations) was employed to obtain thermodynamic parameters.

2.7. Langmuir balance and fluorescence microscopy

Surfactant suspensions were labelled with NBD-PC (ThermoFisher Scientific, 1% mol/mol with respect to phospholipid) for 1 h at 45 °C with orbital agitation. Then, surfactant suspensions were deposited on the air-liquid interface defined by a Langmuir trough 302RB/D1 (Nima Technology) to reach a surface pressure of 2–3 mN/m. Then, monolayers were equilibrated for 15 min and compressed at 25 cm^2/min to obtain pressure-area isotherms while transferring the interfacial film onto delipidized glass coverslips as described elsewhere [39]. An epifluorescence microscopy (Leica DM 4000B), equipped with an ORCA R2 10,600 camera (Hamamatsu, Germany) and L5 Leica filter sets (excitation range 440–520 nm, emission at 497–557 nm), was employed for imaging. ImageJ was used for quantitative measurements.

2.8. Captive bubble surfactometer

Surface activity of the different samples was assessed using a captive bubble surfactometer [40]. The set-up consists of a temperature-controlled chamber containing a buffer solution (Tris 5 mM, NaCl 150 mM, 10% sucrose, pH 7). The air-liquid interface is defined by an air bubble trapped against an agarose cap which encloses the experimental chamber. Our protocol consisted of five consecutive steps. First, a surfactant sample prepared at 12 mg/ml was injected directly close to the air bubble to monitor adsorption for 5 min. Then, the bubble was subjected to a quick expansion to study surfactant spreading and post-expansion adsorption. Next, slow quasi-static and rapid dynamic compression-expansion cycles mimicking breathing rates were sequentially performed. Finally, the bubble was compressed to a minimal volume to evaluate stability once subjected to mechanical perturbations using a pendulum hammer as described [41]. Surface tension was continuously monitored via bubble dimensions using a dedicated software [42].

3. Results

To harvest LS subfractions, the material purified from bronchoalveolar lavages of porcine lungs, termed Native Surfactant (NS) in this work, was divided into seven fractions, termed N1 to N7 by increasing density, via sucrose density gradient (Fig. 1). NS subfractions contained different amounts of surfactant proteins and cholesterol (Fig. 2). In this regard, SP-B and SP-C were detected in N1 to N4 whereas SP-A was predominantly associated with N3 to N5 and N7 (Fig. 2a). Furthermore, N1 and N5 to N7 contained higher cholesterol levels (Fig. 2b). In contrast, NS subfractions comprised similar amounts of saturated and unsaturated molecular species of phosphatidylcholine (Fig. 2b). Then, we performed transmission electron microscopy experiments to study the membranous assemblies included into each of these NS subfractions (representative images included into Figs. 3 and 4). N1, N2 and N3 were apparently constituted by multilamellar assemblies (Fig. 3) whereas N5 to N7 were comprised by polymorphic membranes (N5), multi-vesicular bodies (N6) and lipid/protein aggregates (N7) (Fig. 3). The example of membranous assembly observed in N4 reminded the lattice-shaped structure of tubular myelin. Furthermore, these different membranous assemblies were also observed in NS micrographs, discarding the possibility of being artifacts due to fractionation (Fig. 4).

Next, we evaluated the level of membrane hydration in the different fractions using the extrinsic fluorescence probe Laurdan and assessed the lipid order by ESR. Laurdan is a fluorescent probe highly sensitive to hydration and useful to evaluate lipid packing in phospholipid bilayers and monolayers [36,43]. This is because the maximum of fluorescence emission of Laurdan switches from 440 to 490 nm due to dipole relaxation processes occurring as a consequence of the increase in hydration at the headgroup region of membranes as temperature increases (Fig. 5a). Our experiments showed no differences in the thermotropic profile of Laurdan fluorescence among NS subfractions (Fig. 5b), which reflected ordered-to-disordered phase transitions centered at around 32 °C (calculated from Fig. 5b). Then, we studied how this thermotropic transitions affect the acyl chain molecular mobility as assessed by electron spin resonance using 5 and 12-PCSL spin probes included into the different NS subfractions (Fig. 6). We also aimed to evaluate lipid order at different depth within the membrane plane [37,38,44]. To do so, we calculated the outer hyperfine splitting constants ($2A_{max}$) from all spectra as indicated in Fig. 6a. Our results showed a decay in $2A_{max}$ from 25 to 45 °C in experiments using 5-PCSL, whereas similar $2A_{max}$ values were obtained at all temperatures for NS subfractions including 12-PCSL. From a comparative point of view, no differences were observed among NS subfractions either using 5 or 12-PCSL. Additionally, the thermotropic behaviour of NS subfractions was studied by differential scanning calorimetry (Fig. 7). As observed in Laurdan experiments, a predominant phase transition at temperatures around 30 °C was observed in NS subfractions (Fig. 7). However, N3 exhibited additional contributions at higher temperatures.

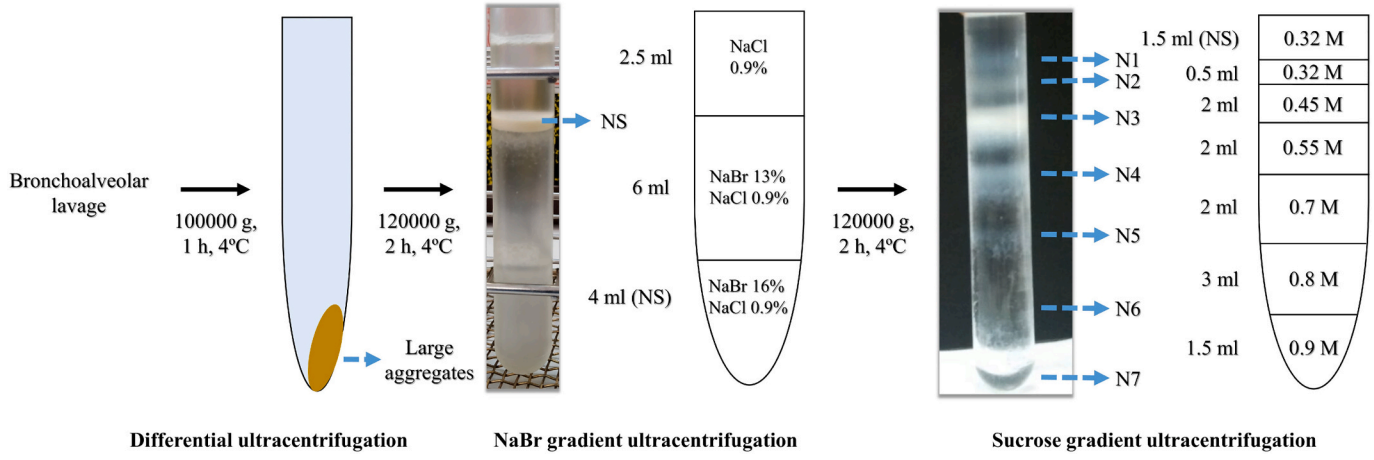

Fig. 1. Purification of NS from bronchoalveolar lavage and its subfractions by density gradient ultracentrifugation. Cell-free bronchoalveolar lavages were subjected to differential ultracentrifugation (100,000 *g*, 1 h, 4 °C). Then, pellets containing full surfactant were loaded into sodium bromide gradients and subjected to density gradient ultracentrifugation (120,000 *g*, 2 h, 4 °C) to obtain NS, which was harvested from the interface between gradient solutions containing NaCl 0.9% and NaCl 0.9% NaBr 13%. Finally, NS subfractions were isolated by sucrose gradient ultracentrifugation (120,000 *g*, 2 h, 4 °C). The images show the result of the centrifugation of whole LS in sodium bromide and of the purified LS into the sucrose density gradient. The schemes represent the volumes and concentrations of each of the solutions used to build the density gradient.

a

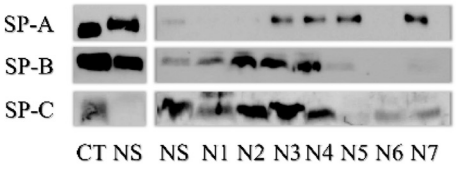

b

	N1	N2	N3	N4	N5	N6	N7	NS
% sat. PC	51.4	46.5	49.1	51.8	46.5	60.5	52.3	51.8
% unsat. PC	48.6	53.5	50.9	48.2	53.5	39.5	47.7	48.2
sat. PC / unsat. PC	1.1	0.9	1.0	1.1	0.9	1.5	1.1	1.1
Phospholipid / Cholesterol	4.3 ± 1.1	14.4 ± 7.5	19.3 ± 3.3	12.5 ± 5.4	6 ± 5	1.1 ± 0.4	2.6 ± 2	24.7 ± 0.6

Fig. 2. Compositional analysis of NS subfractions. (a) Western blot against pulmonary surfactant proteins SP-A, SP-B and SP-C. Equivalent phospholipid amounts were loaded per well. (b) Lipidomic analyses (N = 1) and phospholipid/cholesterol weight ratios (mean value and standard deviation for two replicates) in the different LS subfractions.

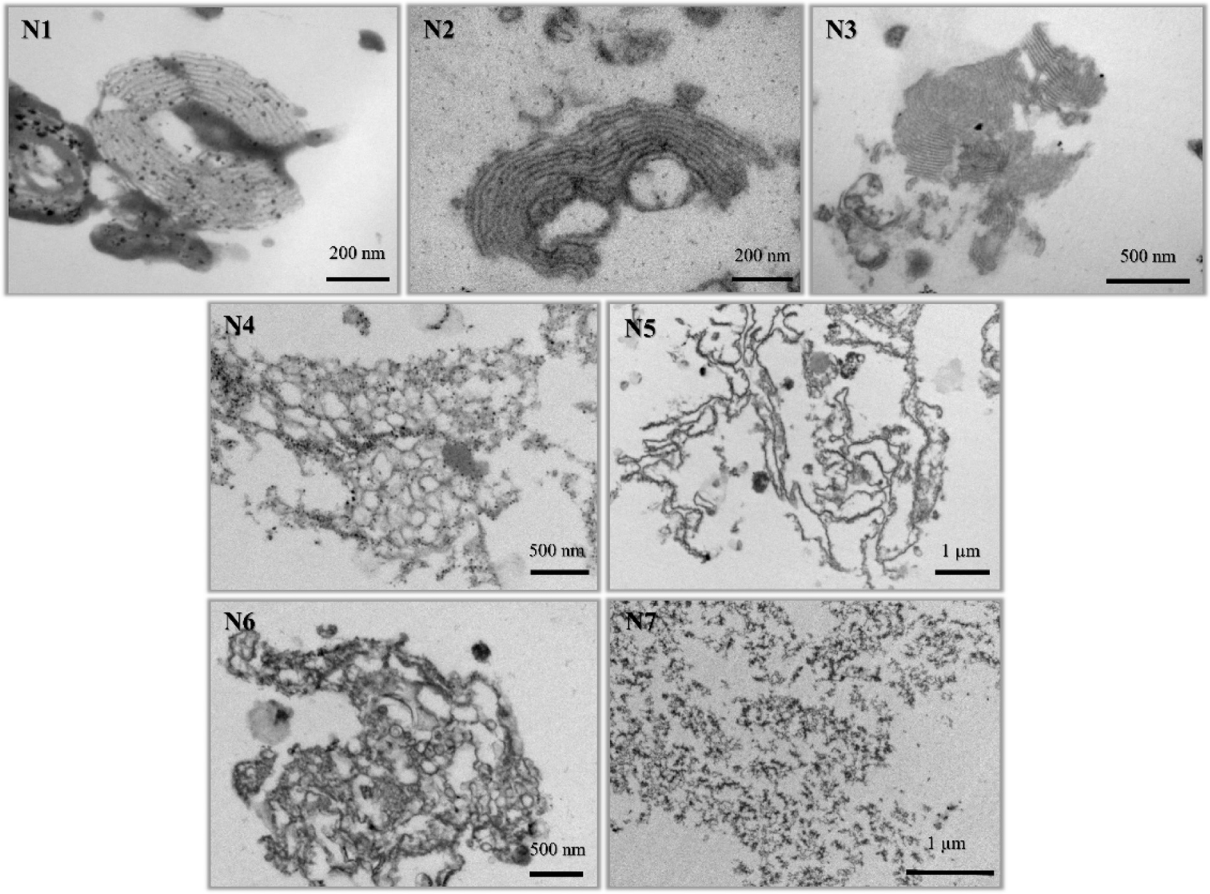

Fig. 3. Analysis by transmission electron microscopy of the structure of surfactant subfractions. An illustrative TEM image is presented from each of the subfractions. N1, N2 and N3 are constituted by multilamellar membranous assemblies. A lattice-shaped lipid structure is observed in N4. Unpacked membranous assemblies, vesicles, and lipid/protein aggregates are observed in subfractions N5, N6 and N7.

To complement the structural study of surfactant assemblies, we performed experiments to evaluate the structure of interfacial films formed by the NS subfractions (Figs. 8 and 9). The samples were labelled with NBD-PC, a lipid-based fluorescent probe that preferably partitions into disordered-like regions. Labelled subfractions were deposited as aqueous suspensions on the air-liquid interface of a Langmuir trough and the formed interfacial films were subjected to compression (Fig. 8) and simultaneously transferred to glass coverslips for observation under an epifluorescence microscope (Fig. 9a). NS subfractions formed similar interfacial films, constituted by a disordered-like phase and containing label-free segregated regions or domains at low surface pressure (below 20 mN/m) (Fig. 9a, black arrows). Upon compression, label-free regions disappeared while label-enriched structures were generated (Fig. 9a, green arrows) accounting for 4–8% of surface area (Fig. 9b). The transition of label-free to label-enriched regions occurred at a surface pressure of around 15 mN/m in NS subfractions (Fig. 9b) except for N3, where label-free structures were observed until 25 mN/m and occupying two-times more area.

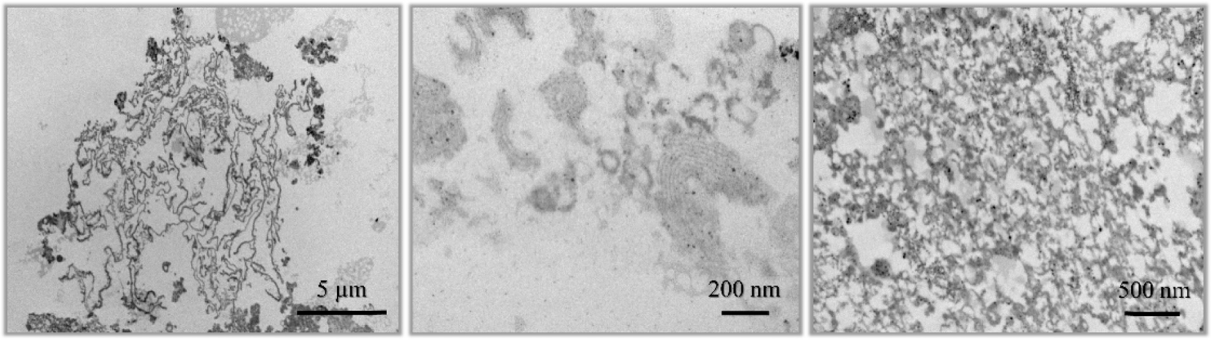

Fig. 4. Structure of whole NS as visualized by transmission electron microscopy. Representative TEM images are presented to illustrate the presence in LS of flexible lipid organizations (left), multilamellar membranous assemblies (middle) and lipid/protein aggregates (right).

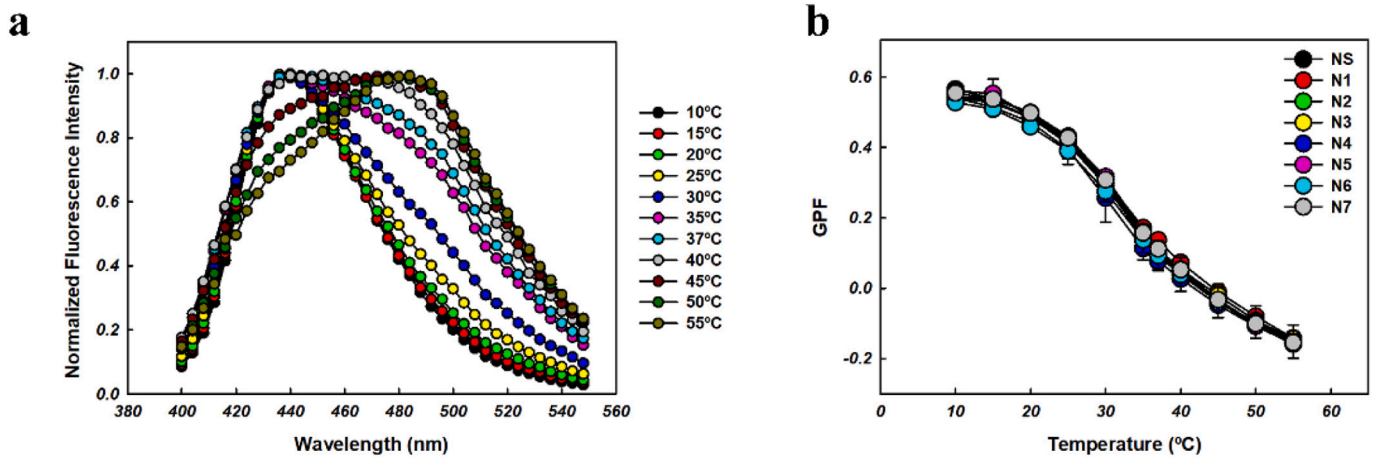

Fig. 5. Hydration of membranes in NS subfractions as sensed by the fluorescent extrinsic probe Laurdan. a) Fluorescence emission spectra recorded for a Laurdan-labelled sample of NS at 10, 15, 20, 25, 30, 35, 37, 40, 45, 50 and 55 °C. b) GPF of Laurdan-labelled NS and its subfractions as a function of temperature. Data correspond to the mean GPF and standard deviation for three replicates.

Finally, we used a captive bubble surfactometer to evaluate and compare the surface activity of the different NS subfractions under conditions mimicking breathing dynamics (Fig. 10 and Table 1) [40,42,45]. Except for N5, NS subfractions adsorbed efficiently into an air-liquid interface in static conditions or after a quick surface area expansion (Fig. 10a), to produce equilibrium surface tensions (γ_{eq}) of around 22 mN/m (Table 1). Moreover, NS subfractions were able to reduce γ to minimal values (around 2 mN/m) from the first quasi-static compression-expansion cycle, though requiring in some cases larger area reduction (Fig. 10b and Table 1). During the subsequent cycles, hysteresis and the percentage of compression required to reach minimal γ were reduced to eventually needing only 20% of area reduction. As it occurred with adsorption, the fraction N5 did not perform an efficient surface activity, i.e. minimal γ values of 10 mN/m with very large percent of area reduction (around 75%) (Fig. 10b and Table 1). Upon breathing-like compression-expansion rates, NS subfractions similarly diminished γ with limited area reduction and no hysteresis (Fig. 10 and Table 1) except for N5. Finally, NS subfractions exhibited comparable stabilities against mechanical perturbations (Table 1).

4. Discussion

Animal-based lung surfactant preparations are the reference for both research and biomedical applications [46]. However, as a result of being subjected to breathing dynamics, these surfactant preparations have been likely exposed to compositional and structural remodelling processes occurring at the alveolar spaces. This may explain why isolated LS complexes comprise very different membranous assemblies [13,25,29,47–51]. The surface-active materials studied here likely include both functional, the so-called large aggregates, and inactive constituents, known as small aggregates [13–16,20]. LBs, LBPs, multibilayer stacks and tubular myelin are observed in large aggregates whereas small vesicles and lipid/protein aggregates typically constitute small aggregates [13]. The distinct surface activity exhibited by large and small aggregates has been attributed to the fact that SP-A, SP-B and SP-C are mainly present into the large aggregates [15,16,52,53]. Indeed, small aggregates are thought to be generated from the large aggregates as a consequence of surface dynamics [14].

According to the results of the present work, we propose that a LS isolated from bronchoalveolar lavages of porcine lungs comprise a heterogeneous mixture of membranous entities beyond the simplistic distinction between large and small aggregates. We suggest that these lipid/protein assemblies may stand for different steps of the biostructural cycle of LS established from its unpacking, once secreted and subjected to respiratory dynamics, to recycling. Our fractions N1-N4, containing all the proteins and constituted by complex multilamellar structures may represent the “large aggregates”, while fractions N5-N7 could represent discrete assemblies typically resolved as “small aggregates” under other fractionation procedures. It therefore seems that the presence of the proteins may be taken as a molecular marker of the most active surfactant structures constituting the large aggregates, and in particular the presence of protein SP-B, in substantial proportion in fractions N1-N4 and practically absent in N5-N7.

It is noteworthy that LBPs represent the original intact membranous

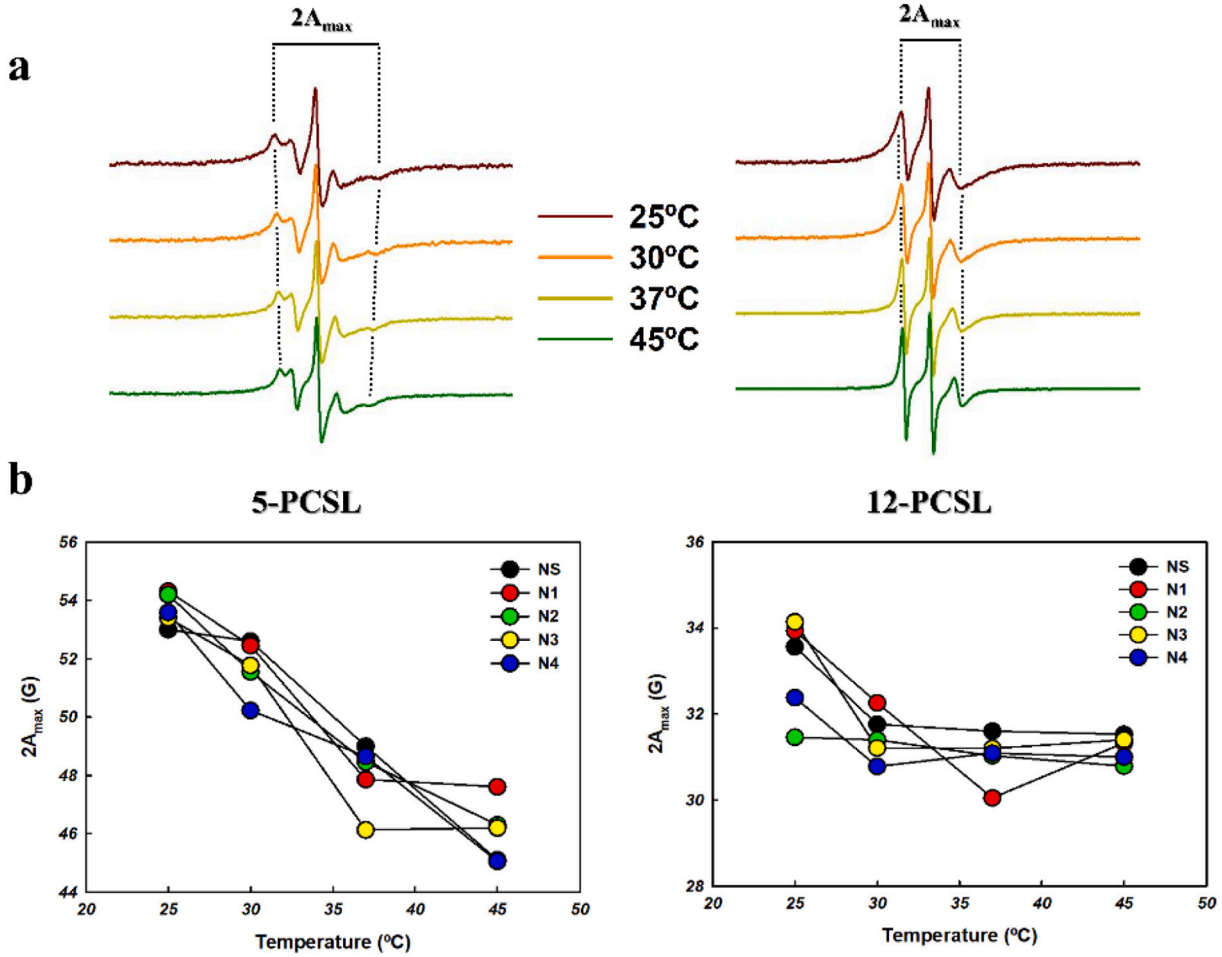

Fig. 6. Mobility and lipid order in NS subfractions as analysed by ESR. a) Illustrative electron spin resonance spectra recorded for a NS sample including a 5-PCSL (left) or 12-PCSL (right) spin probe at 25, 30, 37 and 45 °C. b) Two spectra were accumulated per sample and temperature to minimize signal-to noise ratio. b) $2A_{max}$ was calculated from the spectra as indicated in (a) and plotted as a function of temperature. Subfractions N5, N6 and N7 were not tested due to limitations in sample amounts.

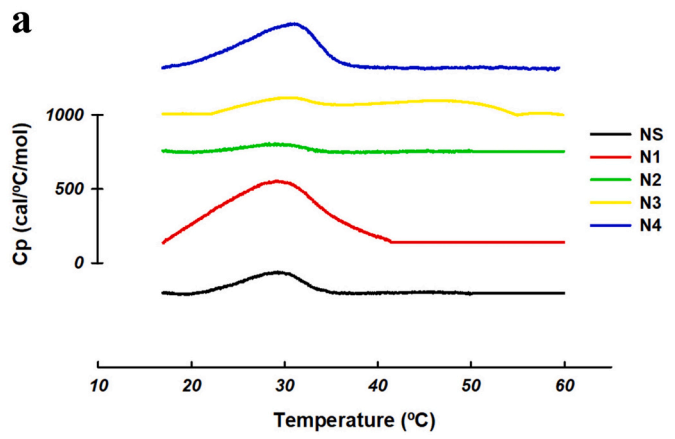

b

Sample	*ΔH (kcal/mol)*	*T_m (°C)*	*$ΔT_{1/2}$(°C)*
NS	1.07	29	7.2
N1	4.8	29.3	12.4
N2	0.3	28.3	6.5
N3	2.3	30.6	26.5
N4	2.9	31	9.1

Fig. 7. Thermotropic behaviour of NS subfractions as analysed by differential scanning calorimetry. a) Illustrative DSC calorimetric thermograms after several replicas of whole NS and its subfractions. b) 15 thermograms were recorded for each sample and the last one was used to calculate thermodynamic parameters associated to ordered-to-disordered transitions.

entity of LS, immediately after the secretion of LBs. As a matter of fact, LBPs are considered to sustain a highly energetic pre-assembled state, result of massive lipid accumulation and compaction attained during LS biogenesis in the LBs [5,6,24,54]. Indeed, LBPs have been described as highly packed and dehydrated membranous assemblies and possibly containing non-lamellar lipid phases [5,6,23]. These freshly secreted assemblies adsorb into the alveolar air-liquid interface, in a process mediated by peripherally located SP-B and SP-C, forming solid-like

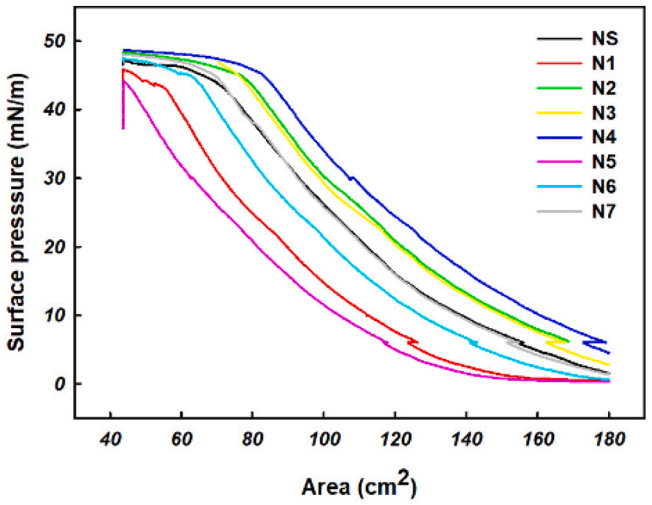

Fig. 8. Compression pressure-area isotherms of interfacial films formed by NS and its subfractions at 25 °C. Mass of phospholipid injected were: 40 μg for NS, 72 μg for N1, 27 μg for N2, 13 μg for N3, 35 μg for N4, 100 μg for N5, 80 μg for N6 and 100 μg for N7.

three-dimensional interfacial films [24,54]. However, the membrane structure and surface activity of LS complexes isolated from operational animal lungs, via bronchoalveolar lavages, is not comparable with those reported for LBPs structures in the literature [5,54], though LBPs are occasionally observed in lavage samples.

The aim of our study was thus 1) fractionate porcine LS into subfractions through sucrose density gradient, for 2) conducting a detailed characterization of the membrane structure and activity of surfactant subfractions in order to identify the potential presence of LBPs in amounts that could allow a detailed characterization of the unique structure-function determinants of freshly secreted, unused, surfactant.

Our starting material was likely enriched in large aggregates of a porcine LS, since larger centrifugation times are required to collect the full fraction of small aggregates. However, our NS possibly also contains part of the original small aggregates in the lavage, or at least some small-like aggregates that are somehow associated with the large ones. We observed that seven different fractions could be distinguished according to density differences (Fig. 1). This suggests that the so-called "large aggregates" fraction is far from homogeneous and contains several coexisting membranous entities. We have found that not only did surfactant proteins partition differently among NS subfractions (Fig. 2a), but they also contained different cholesterol amounts (Fig. 2b). Cholesterol plays major roles determining both lipid phase segregation and fluidity, both affecting the surface activity of LS [2,3,28,46,55–58]. We hypothesize that the less dense NS subfractions (N1-N4) are formed as a result of cholesterol depuration from predominant subfractions during surface dynamics. This may explain why N1, N2, N3 and N4 comprised multilamellar membranous entities whereas N5, N6 and N7 were constituted by small lipid vesicles or aggregates (Figs. 3 and 4), perhaps as a result of their segregation from the largest, depurated, and more active, structures.

We suggest that the variety of membranous assemblies observed in NS subfractions represent different stages during the lifetime of surfactant at the alveolar airspaces, from its secretion to its recycling. Thus, fractions N1 and N2 could represent early states after LS biogenesis, N3 and N4 could include structures formed and evolved during adsorption and breathing cycling, while N5, N6 and N7 could include somehow close to exhausted structures, already spent, and partially targeted for recycling. The presence of protein SP-A into fractions N5 and N7 could therefore indicate that these fractions may be somehow tagged to recycling by type II cells as previously suggested [59]. Fraction N6, with

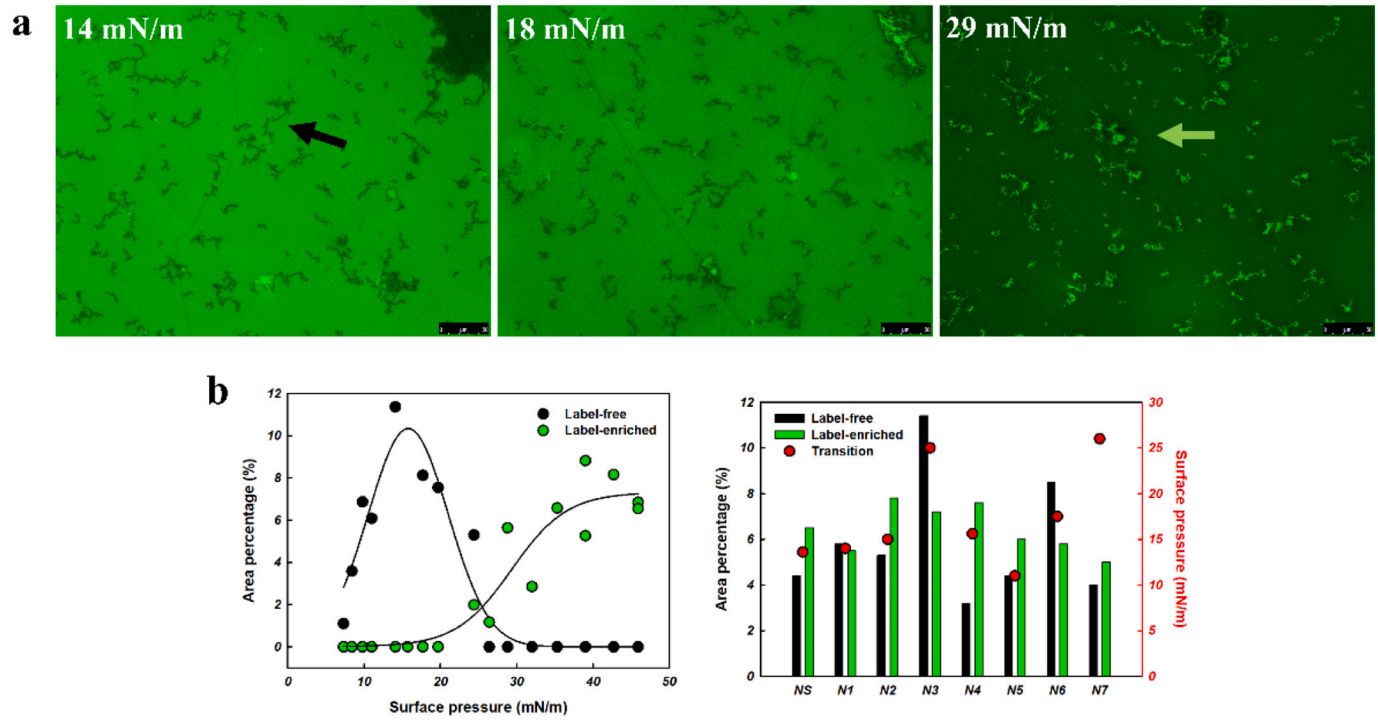

Fig. 9. Lateral structure of interfacial LS films subjected to compression as observed by epifluorescence microscopy. a) Illustrative images were taken from interfacial films formed by the N3 subfraction at the three indicated surface pressures (scale bar, 25 μm). Label-free and label-enriched regions are indicated with black and green arrows respectively. b, left) Percent fraction of area and compression-dependent evolution of label-free and label-enriched regions in N3 films. b, right) Surface pressure (red circles) at which label-free regions are not observed and label-enriched regions start to protrude from the interfacial film; and maximum percent area fraction (bars) occupied by either label-free or label-enriched structures in films formed by each of the NS subfractions. (For interpretation of the references to colour in this figure legend, the reader is referred to the web version of this article.)

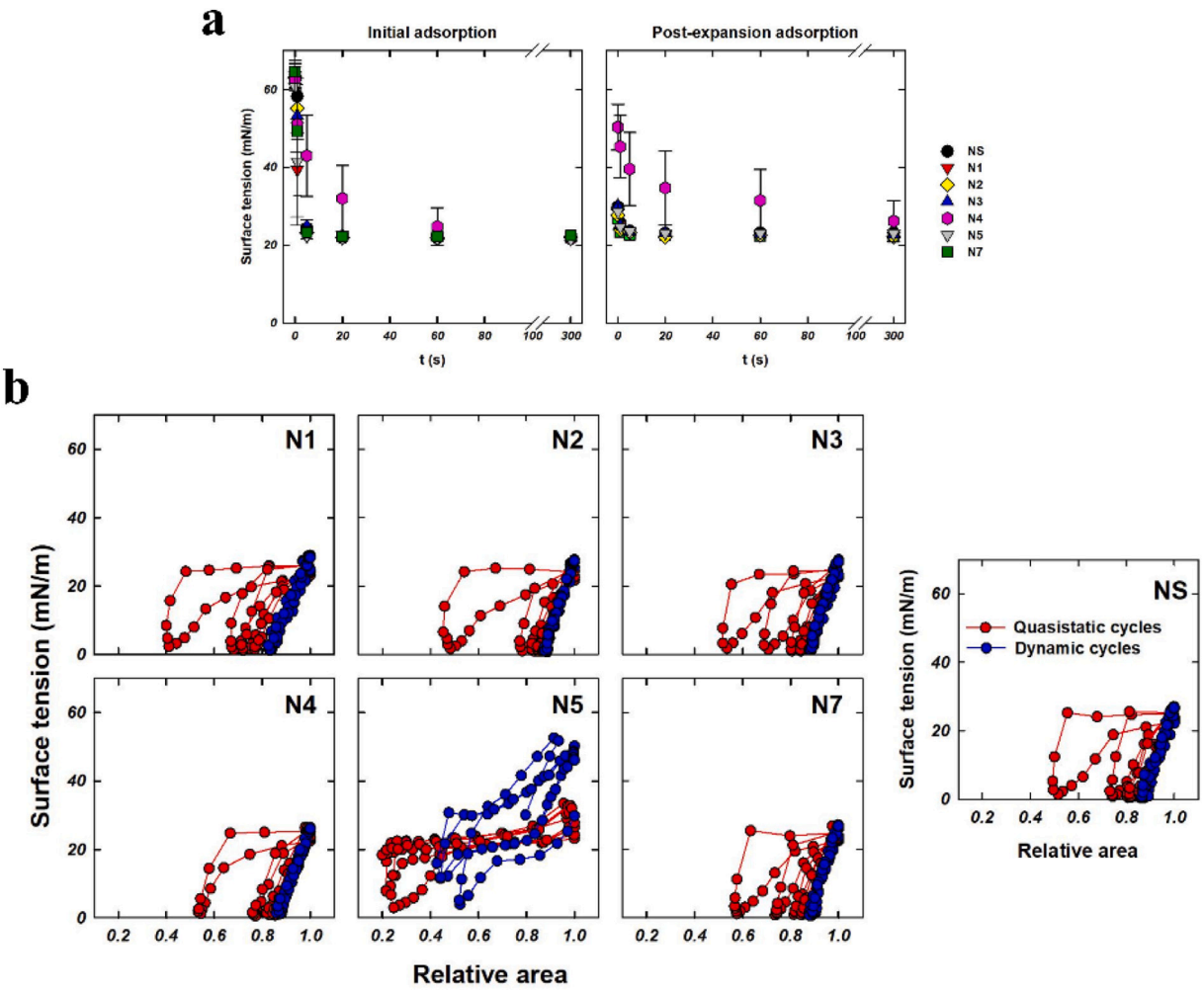

Fig. 10. Surface activity of NS and its subfractions as evaluated in a captive bubble surfactometer. a) Initial interfacial adsorption (left) and after a quick bubble expansion (right). Error bars represent standard deviation after averaging three replicates. b) Isotherms of films formed by the different LS subfractions and whole NS under quasi-static (red) or dynamic (blue) compression-expansion cycling. N6 was not tested due to sample limitation. A representative experiment is shown for each sample. (For interpretation of the references to colour in this figure legend, the reader is referred to the web version of this article.)

no SP-A, could instead be constituted by material to be processed by macrophages. On this basis, we expected subfractions to differ substantially in terms of lipid order and hydration, which are the properties that we found to define more specifically LBPs compared with whole surfactant from lavage [5], beyond the unique morphology of highly packed concentrically arranged bilayers of LBPs. However, and unexpectedly for us, our experiments suggest that all the resolved NS subfractions are constituted by similarly hydrated membranous assemblies with comparable acyl chain mobility along the membrane profile (Figs. 5 and 6). The conclusion, therefore, is that LS purified from lavage is practically devoid of freshly secreted LBPs, likely as a consequence of their full conversion into the observed structures during breathing. Still, the possibility that the particular osmolarity conditions introduced by the sucrose solutions required to prepare the density gradients could have induced some structural effects cannot be fully discarded.

The fact that LS extracted from bronchoalveolar lavages of animal lungs comprises several subfractions with different protein and cholesterol content and micro-structure but with comparable membrane packing is relevant. The results agree with those reported for a NS preparation with or without its native protein and cholesterol content [37], though surfactant proteins and cholesterol have been reported to modify lipid order in different lipid models [44,60,61]. It is remarkable that the calorimetric thermogram of fraction N3 exhibits a broad transition at temperatures above the main phase transition recorded for NS (Fig. 7). We propose that this contribution might be related to the presence of dehydrated DPPC clusters [62] that could be particularly active in sustaining very low surface tension. However, we cannot discard that the transitions observed at those high temperatures could be associated with particular protein-lipid assemblies, or even with structural transitions of the proteins themselves, because fraction N3 is particularly rich in the three surfactant proteins analysed. It is possible that the highly dynamic character of LS complexes when studied as a whole could somehow mask these local, but possibly essential, structural determinants for the surface activity of LS [37]. Similarly, the structure of interfacial films formed by NS subfractions did not differ significantly (Figs. 8 and 9). A predominant disordered-like phase covered the whole interface and only some filamentous label-free regions, especially again in N3, were observed at low surface pressure but disappeared associated with the appearance of excluded structures apparently protruding from the interface (Fig. 9). We speculate that these label-free regions could represent protein-enriched areas allowing monolayer collapse/folding during compression and re-spreading upon expansion. In this line, it has been proposed that the maximization of the interface between condensed and expanded lipid phases in adsorbed films might facilitate monolayer collapse [26,28,63] in a manner that could be modulated by proteins SP-B and SP-C [26,64–69].

Lastly, most of NS subfractions, except N5, had comparable surface activity when assessed in the surfactometer under conditions supposed

Table 1
Parameters defining the functional behaviour of NS and its subfractions tested in the captive bubble surfactometer.

	I. Adsorption	PE. Adsorption	1st Quasi-static			2nd Quasi-static			3rd Quasi-static			4th Quasi-static		
Sample	γ_{eq} (mN/m)	γ_{eq} (mN/m)	γ_{min} (mN/m)	γ_{max} (mN/m)	$AR\gamma_{min}$ (%)	γ_{min} (mN/m)	γ_{max} (mN/m)	$AR\gamma_{min}$ (%)	γ_{min} (mN/m)	γ_{max} (mN/m)	$AR\gamma_{min}$ (%)	γ_{min} (mN/m)	γ_{max} (mN/m)	$AR\gamma_{min}$ (%)
NS	21.7 ± 0.4	23.2 ± 0.1	1.8 ± 0.5	24 ± 0.6	50 ± 4	1.2 ± 0.4	24.2 ± 0.6	27 ± 5	0.9 ± 0.4	24.8 ± 0.4	22 ± 8	0.8 ± 0.3	24.9 ± 0.3	20 ± 7
N1	22.1 ± 0.2	22.3 ± 0.5	2.6 ± 1.2	25.2 ± 0.9	59 ± 6	0.9 ± 0.4	25.7 ± 0.8	33 ± 11	1 ± 0.2	25.4 ± 0.9	26 ± 5	1.1 ± 0.4	25.7 ± 1.2	22 ± 3
N2	22.5 ± 0.9	22.2 ± 0.7	7.4 ± 10.5	24.8 ± 0.4	52 ± 16	1.9 ± 1.9	25.2 ± 1.4	33 ± 24	1.1 ± 0.6	25.7 ± 1	24 ± 14	1.2 ± 0.2	25.1 ± 1	21 ± 10
N3	22.1 ± 0.3	22.3 ± 0.5	2.6 ± 1.1	25 ± 0.6	53 ± 7	1.4 ± 0.3	25.4 ± 0.9	34 ± 4	1 ± 0.1	25.5 ± 0.8	24 ± 5	0.8 ± 0.2	25.6 ± 0.6	20 ± 5
N4	22 ± 0.9	22.7 ± 0.2	3.6 ± 4.1	25.7 ± 0.6	45 ± 20	1.1 ± 0.7	26 ± 0.7	26 ± 14	0.9 ± 0.2	25.9 ± 0.5	21 ± 10	0.7 ± 0.1	25.9 ± 0.5	17 ± 7
N5	24.6 ± 0.4	26.1 ± 5.3	15.6 ± 6.6	26.8 ± 1.8	76 ± 4	13.6 ± 9.2	28.4 ± 4.6	75 ± 1	18.9 ± 0.5	29.5 ± 4.1	76 ± 4	19.2 ± 0.6	31.6 ± 5.4	69 ± 6
N7	21.5 ± 0.7	23 ± 0.4	2.3 ± 1.5	25.4 ± 0.1	57 ± 12	1.5 ± 0.9	25.3 ± 0.4	38 ± 12	1.3 ± 0.4	25.4 ± 0.7	29 ± 12	1.2 ± 0.7	25.9 ± 1.1	24 ± 10

	1st Dynamic			10th Dynamic			20th Dynamic			Stability			
Sample	γ_{min} (mN/m)	γ_{max} (mN/m)	$AR\gamma_{min}$ (%)	γ_{min} (mN/m)	γ_{max} (mN/m)	$AR\gamma_{min}$ (%)	γ_{min} (mN/m)	γ_{max} (mN/m)	$AR\gamma_{min}$ (%)	γ_0 (mN/m)	γ_5 (mN/m)	γ_{10} (mN/m)	γ_{15} (mN/m)
NS	1 ± 0.5	26.9 ± 4.4	14 ± 6	0.7 ± 0.3	27.5 ± 2.2	14 ± 5	0.7 ± 0.4	27.8 ± 1.9	14 ± 4	1.1 ± 0.6	1.9 ± 0.2	3.3 ± 0.5	4.4 ± 0.1
N1	1.4 ± 0.4	26.9 ± 1.4	17 ± 1	1 ± 0.4	28.7 ± 0.6	16 ± 1	0.9 ± 0.4	28.8 ± 0.4	16 ± 1	1.1 ± 0.4	1.7 ± 0.2	2.3 ± 0.1	2.7 ± 0.1
N2	0.9 ± 0.4	28.4 ± 2.5	15 ± 3	0.9 ± 0.4	28.5 ± 2.6	15 ± 3	0.9 ± 0.4	29.4 ± 2.3	15 ± 3	1.7 ± 0.2	2.4 ± 0.2	3.4 ± 0	3.8 ± 0.2
N3	1.3 ± 0.2	27.2 ± 2	13 ± 2	1.2 ± 0.4	27.9 ± 2.3	13 ± 2	1.2 ± 0.4	28.2 ± 2	13 ± 2	1.7 ± 1.2	2.6 ± 0.8	3.6 ± 0.5	4.2 ± 0.6
N4	0.8 ± 0.3	25.2 ± 1.5	14 ± 1	0.9 ± 0.3	26.9 ± 2.8	14 ± 1	0.9 ± 0.4	27.1 ± 2.8	15 ± 2	0.9 ± 0.2	2.1 ± 0.2	3 ± 0.4	3.5 ± 0.6
N5	1.7 ± 1.9	50.1 ± 5.5	47 ± 1	5.8 ± 5.2	54.8 ± 5.7	58 ± 6	9.6 ± 4.9	55.1 ± 7.5	61 ± 5	18.7 ± 2.3	18.3 ± 2.1	18.8 ± 1.7	18.6 ± 2.1
N7	1 ± 0.4	27.2 ± 1.9	16 ± 3	0.9 ± 0.3	28.5 ± 2.2	14 ± 3	0.9 ± 0.3	29.1 ± 2.1	15 ± 2	1.1 ± 0.3	2.2 ± 0.4	3.1 ± 0.5	3.6 ± 0.6

Equilibrium surface tension (γ_{eq}) is shown upon initial and post-expansion adsorption. Minimal surface tension (γ_{min}), maximal surface tension (γ_{max}) and percent of area reduction required to reach γ_{min} ($AR\gamma_{min}$) is presented for each of four quasi-static cycles and for the 1st, 10th and 20th dynamic cycles. For stability, γ_0, γ_5, γ_{10} and γ_{15} are γ after 0, 5, 10 and 15 mechanical perturbations discharged over the bubble by a pendulum hammer. Data correspond to the mean and standard deviation after averaging three replicates.

to mimic respiratory dynamics (Fig. 10 and Table 1): quick adsorption into an air-liquid interface, γ reduction to minimal values with limited area reduction during physiological-like compression-expansion cycling and high mechanical stability. Altogether, the functional properties of NS subfractions did not differ significantly except for N5, which exhibited poor surface activity. That low activity is likely associated with a combined lack of surfactant proteins, particularly SP-B, and the excess of cholesterol, a component whose presence in excessive proportion has been associated with surfactant inactivation [55].

It has been proposed that some physiological mechanisms could have evolved to facilitate a rapid adaptation of the lung surfactant system to special demanding respiratory conditions. High respiratory rates, for instance during strenuous exercise, hyperthermia, i.e. during feverish states, and other challenging situations could require a rapid action to adjust surfactant mechanical properties. This has been demonstrated for heterothermic animals, able to breathe normally under rapid changes of their body temperature [70]. The surfactant system of squirrels, bats and marsupial dunnarts has evolved to a very particular lipid composition that can be rapidly adjusted upon incorporation or depletion of cholesterol. It is to be investigated how different structures in surfactant could participate not so much in the primary function of maintaining sufficiently low surface tension but to support such primary function through a properly coupled lipid trafficking and lipoprotein plasticity. We open the possibility that some of the fractions we are revealing here as part of the alveolar surfactant pool, such as for instance our fraction N6, could actually sustain a complementary system of physiological adaptability to particular breathing demands. The characterization of the relationships between these different fractions and assemblies under meaningful physiological constraints is beyond the scope of the current work. However, the application of the fractionation procedures described here to surfactant materials obtained from different patho-physiological models may offer clues on the metabolic and physiological relationships between the different fractions and the processes involved into their interconversions.

To conclude, the main purpose of this work was to characterize the composition, structure and surface activity of LS subfractions in the bronchoalveolar airspaces. We observed that a surfactant already subjected to breathing dynamics contains a variety of membranous assemblies that may reflect sequential stages in LS metabolism. Remarkably, we were not able to identify a subfraction enriched in membrane assemblies sustaining the structural fingerprint of LBPs. A possible explanation may be that LS complexes isolated from animal lungs may be still functional but be constituted by already spent materials, due to the exposure to air spaces and surface dynamics, and therefore lacking the most important structural determinants and functional features of freshly secreted unused LS complexes.

Declaration of competing interest

The authors declare that they have no known competing financial

interests or personal relationships that could have appeared to influence the work reported in this paper.

Acknowledgements

We dedicate this work to Prof. Félix Goñi, in his 70th birthday, to honor his many years of service in promoting Biophysics along the world, and particularly, to generate and potentiate the fruitful community of Spanish biophysicists that we enjoy today. We also dedicate the study to the memory of Prof. José Luis R. Arrondo, another major actor in the development of Biophysics in Spain, who invited us to contribute this article and that sadly passed away recently.

This work has been supported by grants from the Spanish Ministry of Science and Innovation (RTI2018-094564-B-I00), the Spanish Ministry of Education (FPU15/01731) and by the Regional Government of Madrid (P2018/NMT-4389).

References

[1] E. Lopez-Rodriguez, J. Perez-Gil, Structure-function relationships in pulmonary surfactant membranes: from biophysics to therapy, Biochim. Biophys. Acta 1838 (2014) 1568–1585.
[2] J. Bernardino de la Serna, J. Perez-Gil, A.C. Simonsen, L.A. Bagatolli, Cholesterol rules: direct observation of the coexistence of two fluid phases in native pulmonary surfactant membranes at physiological temperatures, J. Biol. Chem. 279 (2004) 40715–40722.
[3] L. Gomez-Gil, D. Schurch, E. Goormaghtigh, J. Perez-Gil, Pulmonary surfactant protein SP-C counteracts the deleterious effects of cholesterol on the activity of surfactant films under physiologically relevant compression-expansion dynamics, Biophys. J. 97 (2009) 2736–2745.
[4] B. Olmeda, M. Martínez-Calle, J. Pérez-Gil, Pulmonary surfactant metabolism in the alveolar airspace: biogenesis, extracellular conversions, recycling, Ann. Anat. 209 (2017) 78–92.
[5] A. Cerrada, T. Haller, A. Cruz, J. Perez-Gil, Pneumocytes assemble lung surfactant as highly packed/dehydrated states with optimal surface activity, Biophys. J. 109 (2015) 2295–2306.
[6] T. Haller, A. Cerrada, K. Pfaller, P. Braubach, E. Felder, Polarized light microscopy reveals physiological and drug-induced changes in surfactant membrane assembly in alveolar type II pneumocytes, Biochim. Biophys. Acta Biomembr. 1860 (2018) 1152–1161.
[7] T. Haller, et al., Tracing surfactant transformation from cellular release to insertion into an air-liquid interface, Am. J. Phys. Lung Cell. Mol. Phys. 286 (2004) L1009–L1015.
[8] J. Perez-Gil, Structure of pulmonary surfactant membranes and films: the role of proteins and lipid-protein interactions, Biochim. Biophys. Acta 1778 (2008) 1676–1695.
[9] M. Martinez-Calle, B. Olmeda, P. Dietl, M. Frick, J. Perez-Gil, Pulmonary surfactant protein SP-B promotes exocytosis of lamellar bodies in alveolar type II cells, FASEB J. 32 (2018) 4600–4611.
[10] R.A. Pinto, J.R. Wright, D. Lesikar, B.J. Benson, J.A. Clements, Uptake of pulmonary surfactant protein C into adult rat lung lamellar bodies, J. Appl. Physiol. 1985 (74) (1993) 1005–1011.
[11] P.A. Stevens, J.R. Wright, J.A. Clements, Changes in quantity, composition, and surface activity of alveolar surfactant at birth, J. Appl. Physiol. 1985 (63) (1987) 1049–1057.
[12] P.A. Stevens, J.R. Wright, J.A. Clements, Surfactant secretion and clearance in the newborn, J. Appl. Physiol. 1985 (67) (1989) 1597–1605.
[13] N.J. Gross, K.R. Narine, Surfactant subtypes in mice: characterization and quantitation, J. Appl. Physiol. 1985 (66) (1989) 342–349.
[14] N.J. Gross, K.R. Narine, Surfactant subtypes of mice: metabolic relationships and conversion in vitro, J. Appl. Physiol. 1985 (67) (1989) 414–421.
[15] R.A. Veldhuizen, S.A. Hearn, J.F. Lewis, F. Possmayer, Surface-area cycling of different surfactant preparations: SP-A and SP-B are essential for large-aggregate integrity, Biochem. J. 300 (Pt 2) (1994) 519–524.
[16] R.A. Veldhuizen, L.J. Yao, S.A. Hearn, F. Possmayer, J.F. Lewis, Surfactant-associated protein a is important for maintaining surfactant large-aggregate forms during surface-area cycling, Biochem. J. 313 (Pt 3) (1996) 835–840.
[17] E. Putman, L.A. Creuwels, L.M. van Golde, H.P. Haagsman, Surface properties, morphology and protein composition of pulmonary surfactant subtypes, Biochem. J. 320 (Pt 2) (1996) 599–605.
[18] T.E. Nicholas, J.H. Power, H.A. Barr, The pulmonary consequences of a deep breath, Respir. Physiol. 49 (1982) 315–324.
[19] P.R. Miles, L. Bowman, J. Tucker, M.J. Reasor, J.R. Wright, Alterations in rat alveolar surfactant phospholipids and proteins induced by administration of chlorphentermine, Biochim. Biophys. Acta 877 (1986) 167–178.
[20] A.M. Brackenbury, et al., Evaluation of alveolar surfactant aggregates in vitro and in vivo, Eur. Respir. J. 19 (2002) 41–46.
[21] R. Higuchi, J. Lewis, M. Ikegami, In vitro conversion of surfactant subtypes is altered in alveolar surfactant isolated from injured lungs, Am. Rev. Respir. Dis. 145 (1992) 1416–1420.
[22] N.J. Gross, Inhibition of surfactant subtype convertase in radiation model of adult respiratory distress syndrome, Am. J. Phys. 260 (1991) L311–L317.
[23] D. Vanhecke, et al., Lamellar body ultrastructure revisited: high-pressure freezing and cryo-electron microscopy of vitreous sections, Histochem. Cell Biol. 134 (2010) 319–326.
[24] N. Hobi, et al., A small key unlocks a heavy door: the essential function of the small hydrophobic proteins SP-B and SP-C to trigger adsorption of pulmonary surfactant lamellar bodies, Biochim. Biophys. Acta 1863 (2016) 2124–2134.
[25] S.L. Young, E.K. Fram, E.W. Larson, Three-dimensional reconstruction of tubular myelin, Exp. Lung Res. 18 (1992) 497–504.
[26] A. Cruz, L. Vazquez, M. Velez, J. Perez-Gil, Effect of pulmonary surfactant protein SP-B on the micro- and nanostructure of phospholipid films, Biophys. J. 86 (2004) 308–320.
[27] A.K. Sachan, J.A. Zasadzinski, Interfacial curvature effects on the monolayer morphology and dynamics of a clinical lung surfactant, Proc. Natl. Acad. Sci. U. S. A. 115 (2018) E134–e143.
[28] H. Zhang, Q. Fan, Y.E. Wang, C.R. Neal, Y.Y. Zuo, Comparative study of clinical pulmonary surfactants using atomic force microscopy, Biochim. Biophys. Acta 1808 (2011) 1832–1842.
[29] M. Ochs, et al., Using electron microscopes to look into the lung, Histochem. Cell Biol. 146 (2016) 695–707.
[30] J.M. Andersson, K. Roger, M. Larsson, E. Sparr, The impact of nonequilibrium conditions in lung surfactant: structure and composition gradients in multilamellar films, ACS Cent. Sci. 4 (2018) 1315–1325.
[31] J. Gil, O.K. Reiss, Isolation and characterization of lamellar bodies and tubular myelin from rat lung homogenates, J. Cell Biol. 58 (1973) 152–171.
[32] G. Rouser, A.N. Siakotos, S. Fleischer, Quantitative analysis of phospholipids by thin-layer chromatography and phosphorus analysis of spots, Lipids 1 (1966) 85–86.
[33] F. Simbari, et al., Plasmalogen enrichment in exosomes secreted by a nematode parasite versus those derived from its mouse host: implications for exosome stability and biology, J. Extracell Vesicles 5 (2016) 30741.
[34] C.C. Allain, L.S. Poon, C.S. Chan, W. Richmond, P.C. Fu, Enzymatic determination of total serum cholesterol, Clin. Chem. 20 (1974) 470–475.
[35] T. Parasassi, G. De Stasio, G. Ravagnan, R.M. Rusch, E. Gratton, Quantitation of lipid phases in phospholipid vesicles by the generalized polarization of Laurdan fluorescence, Biophys. J. 60 (1991) 179–189.
[36] M.V. Picardi, A. Cruz, G. Orellana, J. Perez-Gil, Phospholipid packing and hydration in pulmonary surfactant membranes and films as sensed by LAURDAN, Biochim. Biophys. Acta 1808 (2011) 696–705.
[37] J. Bernardino de la Serna, et al., Segregated phases in pulmonary surfactant membranes do not show coexistence of lipid populations with differentiated dynamic properties, Biophys. J. 97 (2009) 1381–1389.
[38] D. Marsh, Electron spin resonance in membrane research: protein-lipid interactions, Methods 46 (2008) 83–96.
[39] L. Wang, A. Cruz, C.R. Flach, J. Perez-Gil, R. Mendelsohn, Langmuir-Blodgett films formed by continuously varying surface pressure. Characterization by IR spectroscopy and epifluorescence microscopy, Langmuir 23 (2007) 4950–4958.
[40] S. Schurch, H. Bachofen, J. Goerke, F. Possmayer, A captive bubble method reproduces the in situ behavior of lung surfactant monolayers, J. Appl. Physiol. 1985 (67) (1989) 2389–2396.
[41] D. Schurch, O.L. Ospina, A. Cruz, J. Perez-Gil, Combined and independent action of proteins SP-B and SP-C in the surface behavior and mechanical stability of pulmonary surfactant films, Biophys. J. 99 (2010) 3290–3299.
[42] W.M. Schoel, S. Schurch, J. Goerke, The captive bubble method for the evaluation of pulmonary surfactant: surface tension, area, and volume calculations, Biochim. Biophys. Acta 1200 (1994) 281–290.
[43] C.C. De Vequi-Suplicy, C.R. Benatti, M.T. Lamy, Laurdan in fluid bilayers: position and structural sensitivity, J. Fluoresc. 16 (2006) 431–439.
[44] A. Cruz, C. Casals, I. Plasencia, D. Marsh, J. Perez-Gil, Depth profiles of pulmonary surfactant protein B in phosphatidylcholine bilayers, studied by fluorescence and electron spin resonance spectroscopy, Biochemistry 37 (1998) 9488–9496.
[45] C. Autilio, J. Perez-Gil, Understanding the principle biophysics concepts of pulmonary surfactant in health and disease, Arch. Dis. Child. Fetal Neonatal Ed. 104 (2019) F443–f451.
[46] M. Echaide, C. Autilio, R. Arroyo, J. Perez-Gil, Restoring pulmonary surfactant membranes and films at the respiratory surface, Biochim. Biophys. Acta (2017), https://doi.org/10.1016/j.bbamem.2017.03.015.
[47] M. Ochs, The closer we look the more we see? Quantitative microscopic analysis of the pulmonary surfactant system, Cell. Physiol. Biochem. 25 (2010) 27–40.
[48] J. Bastacky, et al., Alveolar lining layer is thin and continuous: low-temperature scanning electron microscopy of rat lung, J. Appl. Physiol. 1985 (79) (1995) 1615–1628.
[49] H. Fehrenbach, Alveolar epithelial type II cell: defender of the alveolus revisited, Respir. Res. 2 (2001) 33–46.
[50] H. Bachofen, U. Gerber, P. Gehr, M. Amrein, S. Schurch, Structures of pulmonary surfactant films adsorbed to an air-liquid interface in vitro, Biochim. Biophys. Acta 1720 (2005) 59–72.
[51] F.R. Poulain, et al., Ultrastructure of phospholipid mixtures reconstituted with surfactant proteins B and D, Am. J. Respir. Cell Mol. Biol. 20 (1999) 1049–1058.
[52] K. Inchley, A. Cockshutt, R. Veldhuizen, F. Possmayer, Dissociation of surfactant protein B from canine surfactant large aggregates during formation of small surfactant aggregates by in vitro surface area cycling, Biochim. Biophys. Acta 1440 (1999) 49–58.

[53] D. Froh, et al., Lamellar bodies of cultured human fetal lung: content of surfactant protein a (SP-A), surface film formation and structural transformation in vitro, Biochim. Biophys. Acta 1052 (1990) 78–89.
[54] A. Ravasio, B. Olmeda, C. Bertocchi, T. Haller, J. Perez-Gil, Lamellar bodies form solid three-dimensional films at the respiratory air-liquid interface, J. Biol. Chem. 285 (2010) 28174–28182.
[55] L. Gunasekara, et al., Pulmonary surfactant function is abolished by an elevated proportion of cholesterol, Biochim. Biophys. Acta 1737 (2005) 27–35.
[56] S. Baoukina, E. Mendez-Villuendas, D.P. Tieleman, Molecular view of phase coexistence in lipid monolayers, J. Am. Chem. Soc. 134 (2012) 17543–17553.
[57] S. Baoukina, D. Rozmanov, E. Mendez-Villuendas, D.P. Tieleman, The mechanism of collapse of heterogeneous lipid monolayers, Biophys. J. 107 (2014) 1136–1145.
[58] E. Lopez-Rodriguez, M. Echaide, A. Cruz, H.W. Taeusch, J. Perez-Gil, Meconium impairs pulmonary surfactant by a combined action of cholesterol and bile acids, Biophys. J. 100 (2011) 646–655.
[59] S.R. Bates, P63 (CKAP4) as an SP-A receptor: implications for surfactant turnover, Cell. Physiol. Biochem. 25 (2010) 41–54.
[60] A. Cruz, D. Marsh, J. Perez-Gil, Rotational dynamics of spin-labelled surfactant-associated proteins SP-B and SP-C in dipalmitoylphosphatidylcholine and dipalmitoylphosphatidylglycerol bilayers, Biochim. Biophys. Acta 1415 (1998) 125–134.
[61] V. Schram, S.B. Hall, SP-B and SP-C alter diffusion in bilayers of pulmonary surfactant, Biophys. J. 86 (2004) 3734–3743.
[62] S. Ohtake, C. Schebor, S.P. Palecek, J.J. de Pablo, Phase behavior of freeze-dried phospholipid-cholesterol mixtures stabilized with trehalose, Biochim. Biophys. Acta 1713 (2005) 57–64.
[63] Y.Y. Zuo, et al., Atomic force microscopy studies of functional and dysfunctional pulmonary surfactant films. I. Micro- and nanostructures of functional pulmonary surfactant films and the effect of SP-A, Biophys. J. 94 (2008) 3549–3564.
[64] S.G. Taneva, K.M. Keough, Dynamic surface properties of pulmonary surfactant proteins SP-B and SP-C and their mixtures with dipalmitoylphosphatidylcholine, Biochemistry 33 (1994) 14660–14670.
[65] A. Cruz, C. Casals, K.M. Keough, J. Perez-Gil, Different modes of interaction of pulmonary surfactant protein SP-B in phosphatidylcholine bilayers, Biochem. J. 327 (Pt 1) (1997) 133–138.
[66] S. Krol, et al., Formation of three-dimensional protein-lipid aggregates in monolayer films induced by surfactant protein B, Biophys. J. 79 (2000) 904–918.
[67] K. Nag, S.G. Taneva, J. Perez-Gil, A. Cruz, K.M. Keough, Combinations of fluorescently labeled pulmonary surfactant proteins SP-B and SP-C in phospholipid films, Biophys. J. 72 (1997) 2638–2650.
[68] K. Nag, J. Perez-Gil, A. Cruz, N.H. Rich, K.M. Keough, Spontaneous formation of interfacial lipid-protein monolayers during adsorption from vesicles, Biophys. J. 71 (1996) 1356–1363.
[69] K. Nag, J. Perez-Gil, A. Cruz, K.M. Keough, Fluorescently labeled pulmonary surfactant protein C in spread phospholipid monolayers, Biophys. J. 71 (1996) 246–256.
[70] L.N. Suri, et al., Adaptation to low body temperature influences pulmonary surfactant composition thereby increasing fluidity while maintaining appropriately ordered membrane structure and surface activity, Biochim. Biophys. Acta 1818 (2012) 1581–1589.